The HERA-B Multi-Target System. (Version 3.0)

U. Dretzler, G. Ernst, K. Ehret [2], C. van Eldik, S. Fricke, M. Funcke, C. Hast, S. İşsever, K. Rudolf, J. Spengler [4], S. Spratte, M. Symalla, D. Wegener

Institute of Physics, University of Dortmund, Germany

V. Aushev [2], V. Pugatch [1,2,4], N. Tkatch [2,4], Y. Vassiliev [2,3]

Kiev Institute of Nuclear Research, Prospekt Nauki 47, 03680,Kiev-28, Ukraine

Abstract

The design and performance of the internal multi-target system operated at the HERA proton storage ring are described. The interaction rate of up to 40 MHz has been produced equally distributed over up to 8 targets which were operated simultaneously in the beam halo. Issues of rate stabilization as well as rate equalization over targets by means of a feedback system are addressed.

Key words: storage ring, internal target, high interaction rate, multi-target steering, rate sharing, rate stabilization

1 Introduction

The HERA – B detector [1] at DESY (Hamburg, Germany) was designed as a forward spectrometer aimed to study heavy-flavor physics in parallel to the other HERA experiments. To reach the goals (among them CP violation in B-mesons decays) one has to provide up to $4 \cdot 10^7$ inelastic interactions per

[1] Correspondence address: DESY, Notkestrasse 85, D-22603 Hamburg, Germany. E-mail address: *Valery.Pugatch@desy.de*

[2] DESY, D-22603 Hamburg, Germany.

[3] Institute of Physics, University of Dortmund, Germany

[4] Max-Planck-Institut für Kernphysik, P.O.B. 103980,D-69029 Heidelberg, Germany

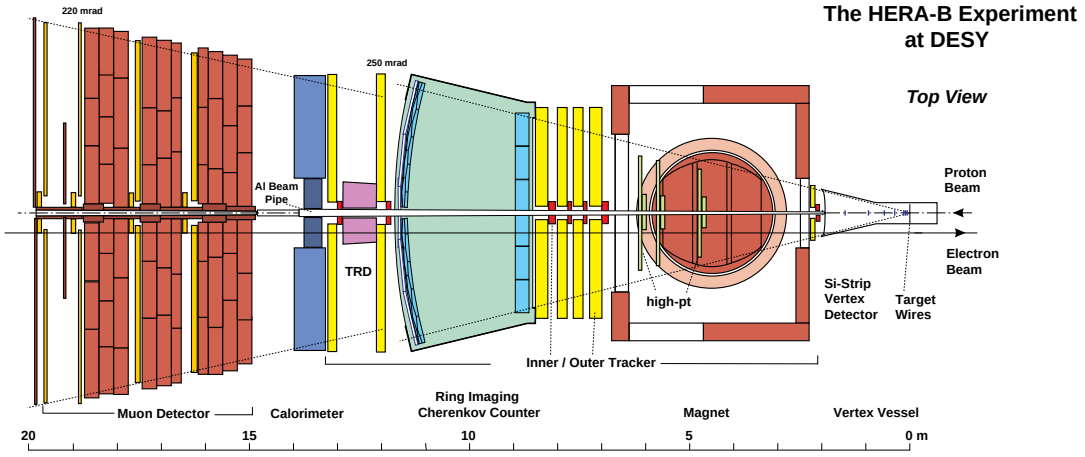

Fig. 1. *Schematic side view of the HERA-B detector. Proton beam hits targets placed inside the Vertex Detector Vessel in UHV environment. Up to eight targets are operated simultaneously at the halo of a beam.*

second for the 920 GeV protons scattered on internal targets with different atomic mass. There are well-known internal target designs for storage rings: gas-jet - [3,2,4], micro-particle-jet- [5] targets, intersecting the whole beam profile, or massive targets operating in the beam halo [7].

In favor of an undisturbed ep-luminosity at other HERA experiments and a good localization of primary vertices at extremely high interaction rate, the HERA – B target has been built as an internal multi-target setup operated in the halo of the HERA proton beam, only. The feasibility of the concept has been demonstrated by a target test setup in 1994 [8]. Since the year 1997 the complete setup with eight targets was operated till the year 2003 nearly continuously at the HERA West Hall.

After a description of internal Multi-Target System basics in section 2 and the experimental set-up in section 3, we present operation experience including the luminosity measurement results in section 4. The article concludes with a summary.

2 Basic Operation Principle and Design of the Internal Multi-Target System.

2.1 Basic Design Criteria.

The internal Multi-Target System (MTS) must fit into physics topics of the HERA – B experiment (Fig. 1) providing cohabitation with other experiments at HERA storage ring [9]. The following design criteria were taken into ac-

count:

- a high interaction rate - up to 40 MHz - for precise measurement of the cross-sections of rare processes;
- up to 8 targets operating simultaneously - for the reliable localization of primary vertices and providing lowest systematic errors in the determination of relative cross-sections;
- equal distribution of the interaction rate over the targets as well as over proton beam bunches - for high efficiency of the vertices reconstruction;
- targets with a mass atomic number ranging from the light to heavy nuclei - for the studies of A-dependence of measured cross-sections;
- targets operating in the beam halo - for providing a cohabitation with other HERA experiments;
- individual target as well overal HERA-B luminosity monitoring;

2.2 HERA Proton Beam

The HERA storage ring at DESY (Hamburg) accumulates 920 GeV protons ($\approx$ 80 mA) and 27 GeV positrons ($\approx$ 30 mA). At its four straight sections it houses four experiments [10]. H1 and ZEUS are the experiments with colliding e-p beams. The HERMES experiment explores the electron beam scattered at an internal polarized gas target whereas the HERA – B experiment utilizes the proton beam scattered at internal multi-wire target. The optics for the west straight section of the HERA was rebuilt to accommodate the HERA – B detector. The beta-function was optimized to minimize the impact of multiple scattering and to allow an unambiguous assignment of reconstructed vertices to a target. The HERA proton collimator system rebuilt at the West Hall [1,11] provided effective shielding of the other experiments [12] from the background borne by HERA – B target operation.

In Tab. 1 the most important parameters of the HERA proton beam at the location of the HERA – B target are summarized.

As far as 180 out of the 220 buckets are filled at HERA the effective proton bunch crossing frequency R_{BX} is given by:

$$R_{BX} = \frac{180}{220} * 1/96 \text{ ns} = 8.52 \text{ MHz}. \quad (1)$$

Thus, 4-5 inelastic interactions per bunch-crossing have to be produced to achieve the HERA-B design interaction rate of 40 MHz. The number of produced interactions per bunch crossing follows the Poisson statistics:

$$p_\mu(n) = \frac{\mu^n}{n!} \exp(-\mu), \quad n = 0, 1, 2, 3, ... \quad (2)$$

HERA-p	x	y
beta function β	35 m	35 m
typical emittance ϵ	$4 \cdot 10^{-9}$rad m	$3 \cdot 10^{-9}$rad m
spatial dispersion η	-470 mm	-1 mm
angular dispersion η'	-13.5 mrad	0
beam size $\sigma_{x\|y} = \sqrt{\epsilon_{x\|y} \cdot \beta_{x\|y}}$	0.35 mm	0.3 mm
beam divergence $\sigma_{x'\|y'} = \sqrt{\epsilon_{x\|y}/\beta_{x\|y}}$	10.5 μrad	9.2 μrad

Table 1
Parameters of the proton beam at the HERA-B target position. The horizontal direction is denoted by the index x, the vertical by y.

where $p_\mu(n)$ describes the probability to get n interactions during one bunch crossing (bx) if the mean number of interactions per bx is μ. As far as the variance of the Poisson distribution is equal to its mean value μ, the number of interactions per bunch crossing gets rather broad.

There are $3 * 6$ bunch trains,each consisting of 10 bunches of $\sim (1-2)$ ns length. The bunch length grows from 1.2 to 2.2 ns during a HERA luminosity run. The bunch spacing within a train corresponds to 96 ns. The bunch length and the its longitudinal stability are important for the experiment (starting point for sub-detector systems). Therefore the bunch length should not exceed 2 ns, otherwise it starts to deteriorate the time resolution. Longitudinal instable protons interacting with the target spoils up the detector and trigger efficiencies. Such an extreme case is illustrated in Fig. 2 underlying the necessity of the bunch population monitoring: for the OUTER-2 target there is no bunch structure visible at all (bottom plot), while for the INNER-1 bunch intensity varies by factor of 3 (upper plot). In such extreme cases the proton fill is by far not efficient for the data taking. The data related to the bunch population were measured each 24 ns by means of the 40 MHz Flash ADC [15–18].

2.3 HERA-B Target Functionality Principle

The functional principle of the HERA-B multi-target system [8] is as follows: protons which leave the beam core, interact on targets which move IN- or OUT- the beam to provide stable interaction rate. Those protons would be lost on an aperture limitation, anyhow. Diffusion and multiple scattering are the main processes which determine the efficiency to catch up protons by the target. The proton ring is operated at typical currents of $I_{\rm p} \approx 80\ mA$ and reaches natural lifetimes $\tau_{\rm nat}$ close to thousand hours. This results in a natural

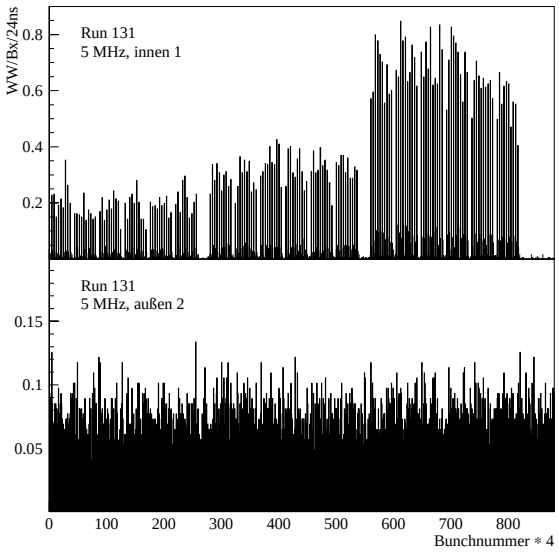

Fig. 2. *Bunch population as seen by different targets (OUTER-2 and INNER-1). Interaction rate produced during the first 24 ns of every bunch was measured by the FADC and is shown as a function of the bunch number.*

proton loss rate of:

$$R_{\text{loss}} = \frac{I_{\text{p}}}{e}\frac{t_{\text{turn}}}{\tau_{\text{nat}}} \approx 3 \text{ MHz} \tag{3}$$

Here the t_{turn} (21.12 μs) is the time the protons need to make a full turn through the ring. The small loss rate (Eq. 3) indicates that high interaction rates cannot be achieved by means of the natural diffusion: the target has to scrape additional protons out of the beam halo. This reduces the lifetime of the beam significantly (less than $\approx$ 80 hours). To achieve a high target efficiency ϵ_T (the ratio between the target interaction rate and the total HERA proton loss rate) an efficient competition of the target with the collimators is needed. The target acts like a semi-transparent collimator. The proton density outside of the target is reduced and just a small number of protons gets lost on the aperture limitations.

Protons have to hit a 500 μm long target several hundred times before an interaction takes place (cf. Tab. 2). The number $N(t)$ of target hits after t revolutions can be estimated by calculating the spatial probability density of a particle with a betatron amplitude W which is larger than the betatron amplitude T which corresponds to the target location. In the horizontal plane e.g. the particle oscillates with the betatron phase $\phi_x(t)$: $x(t) = W_x \cdot \sin\phi_x(t)$. Since the tune Q_x is not a rational number, the phase randomizes and the probability dN/dt that the target with a horizontal width δ_x is hit in one revolution can be approximated by:

$$dN/dt \approx \delta_x/(\pi\sigma_x\sqrt{W^2 - T^2}) \approx (10^{-2}). \tag{4}$$

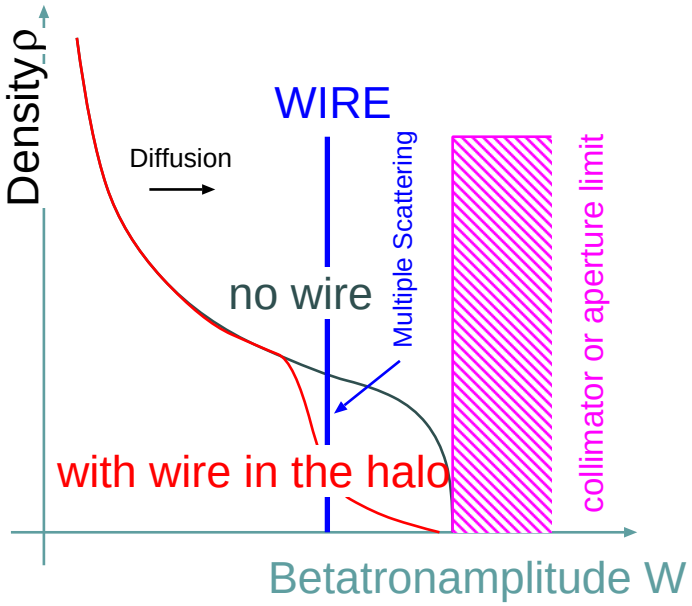

Fig. 3. Schematic view on a halo target illustrating the basic impacts .

Here δ_x is usually 50 μm, the beam width $\sigma_x \approx 400\mu$m. Detailed simulations lead then to values of several ten-thousand up to a few hundred-thousand turns before a proton interacts in the target after its first hit on the target. Thus, a proton in the vicinity of the target has a typical lifetime in the order of a second [8,26]. Diffusion processes have a similar time scale. Typical drift velocities are in the range of 0.1 to 10 σ/s and increase very steeply with the betatron amplitude W. The total angular smearing due to multiple scattering before a proton interacts in the target is given by:

$$\Theta_{sc}^2 \approx \left(\frac{14\text{MeV}}{p}\right)^2 \cdot \frac{\lambda_{int}}{X_{rad}} \tag{5}$$

where p is the momentum of the particle. Comparing this number (Tab. 2) with the beam divergence $\sigma_{x'|y'}$ (Tab. 1) shows that this leads to an effective blow up of the betatron amplitude of several σ. This widening of the beam due to multiple scattering is the main limitations in the HERA – B environment. Therefore a reasonable large aperture is required to achieve anticipated target efficiency $\epsilon_T \approx 50$ %. Results of detailed simulation, showing that one needs around two to three σ distance between the target and the aperture limitation, are confirmed by all measurements. While collimators at HERA are positioned at around 6 beam σ the target wires operate at a typical distance of (3 - 4) σ from the beam center [20–22].

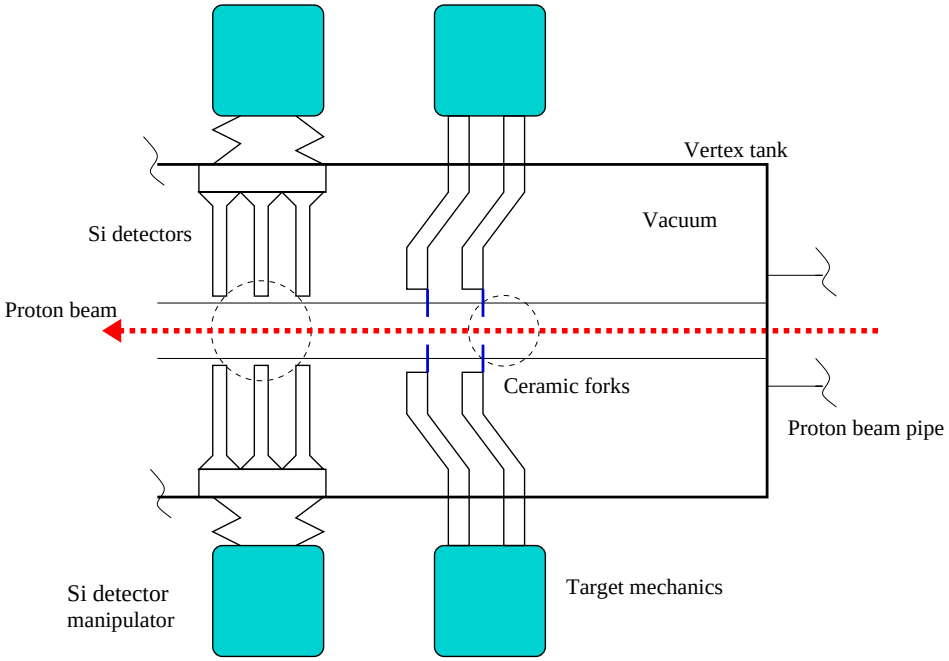

Fig. 4. *Sketch of the Target mechanics mounted at the VDS vessel.*

3 HERA – B Target Setup

3.1 Target Mechanics

To keep the interaction rate stable the target mechanics has to move targets in small steps (typically ≈ 1 μm) in- and out- the halo of the proton beam. It uses a set of 8 targets - either thin round wires (diameter 50 μm) or ribbons (50 x 500 μm). They are mounted and operated in two stations separated by approximately 4 cm along the beam axis. Within one station four different targets are located at nearly equal z-position and approach the beam from four sides. A wear-out of all movable parts was minimized to allow a reliable and continuous operation of the mechanics [22].

The mechanics (sketched simplified in Fig. 4) is mounted at the vacuum vessel which houses the HERA – B Vertex Detector System (VDS) [23]. Protons come from the right side through r/f shielding rod (stainless steel) mounted at the VDS vessel entrance window and reach the targets inserted in a beam halo by linear motor stages ('Target Mechancis'). A special shape of the target forks supporting target-wires is needed to reach as close position to the VDS superlayers as possible. The first three superlayers of the silicon vertex detector are indicated in Fig. 4 together r/f shielding bands (7 μm thick stainless steel foils, ≈ 2 m long) on the right side from the targets. To minimize the impact onto the proton beam dynamics targets are housed in a stainless steel cages welded at the end of the r/f shielding rod.

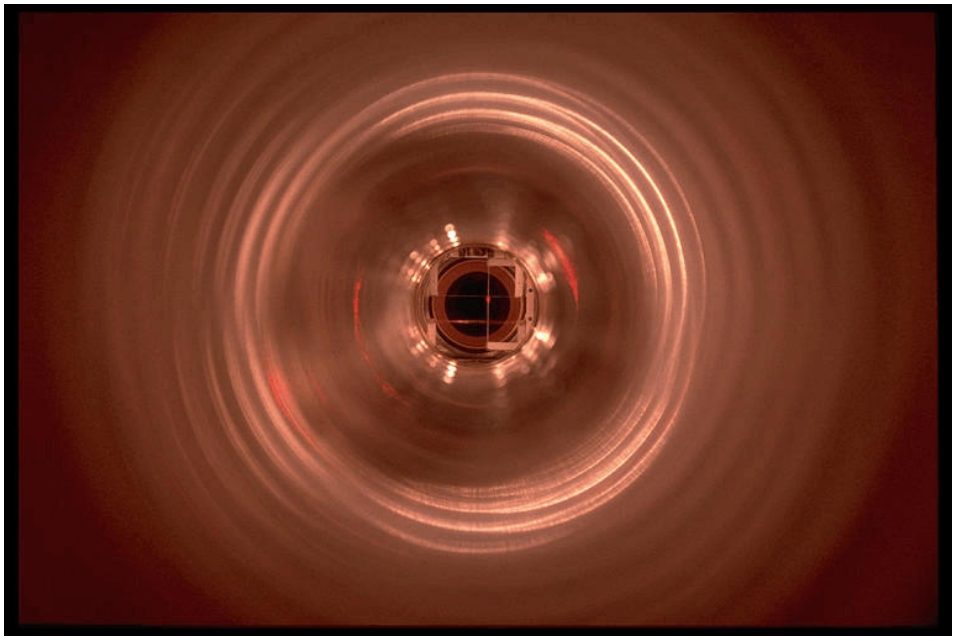

Fig. 5. *Photo of 3 targets supported by ceramics forks moved in a close to proton beam position by target mechanics mounted at the VDS vessel. The laser spot is visible at the crossroad of the 'above' and 'outer' targets. Reflections of the light in a shape of rings occur at the r/f shielding pipe which ends up with stainless steel cages housing all eight targets. The proton beam enters the target setup in the same direction.*

Fig. 5 depicts 3 targets (inserted from all side but from the left) enlightened by a laser light from the entrance window of the Vertex Detector Vessel.

The main attributes of mechanics built on a modular basis include:

- mounting and operation of eight targets in UHV environment, close to the p-beam line;
- the μm range for the precision and the clearance fit;
- stepping motors (50 nm step), sledges, spindles;
- target forks for mounting electrically isolated targets;
- cables, vacuum feedthroughs, end-switches;
- alignment provided by mechanical survey and reconstructed vertices;
- reliability, safety, reproducibility, long-term stability;

More detailed view of one out of four HERA-B target stations is shown in Fig.6.

The choice of the target material and geometry has to accomplish several goals while paying attention to certain constraints. Table 2 summarizes properties of selected target materials. Light target materials are in the multiple scattering dominated environment at HERA – B more advantageous to achieve a high target efficiency (cf. Eq: 5). In case of limitation due to halo diffusion one

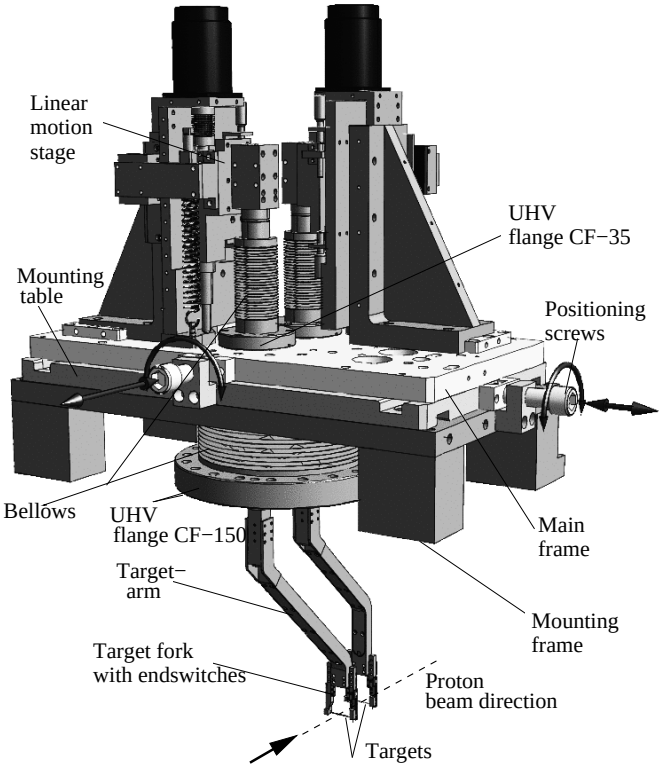

Fig. 6. *A single Target mechanics station mounted at the VDS vessel. Each target station operates two targets.*

would aim for more or heavier material in order to catch up the halo protons faster. The final HERA – B physics program aimed at the A dependence and requested therefore different materials with a high purity from very light to heavy with large lever arms between the individual materials. Other criteria for the target material selection (in addition to the physics one) are the mechanical stability, rigidity and a high melting point.

The multi-target feedback system requires a conductive target material to perform the measurement of the individual target rate by means of acharge integrator connected to the electrically isolated target (cf. Sect. 3.3). The dimensions are chosen in such a way that the geometrical defined location of

Table 2
Atomic number Z, mass A, interaction length λ_{int}, radiation length X_{rad} and mean angular smearing Θ_{sc} at 920 GeV for various target materials (as determined by Eq. 5)

Material	C	Al	Ti	Fe	Cu	Pd	W
Z	6	13	22	26	29	46	74
A	12.	27.	47.9	55.9	63.6	106.4	1 84.9
λ_{int}/cm	38.1	39.4	27.5	16.8	15.1		9.6
X_{rad}/cm	18.8	8.9	3.56	1.76	1.43		0.35
Θ_{sc}/μrad	23.	34.	45.	49.	52.		8 0.

the main interaction vertex on the target is smaller than the expected vertex resolution ($\approx$ 25 μm in transversal direction and $\approx$ 500 μm in longitudinal direction) of the HERA – B detector. The heat development inside the target caused by the energy loss of the penetrating protons limits the target size by $\approx$ 10 μm. Besides an unlike permanent high temperature this would incorporate the danger to melt the target even in a short rate spike. The used targets were made out of carbon, aluminum, titanium, copper, iron, palladium and tungsten.
Since the operation of motors, gears and other movable mechanical parts in UHV would introduce additional complications to the system, all parts of the mechanics that provide the movement of the targets and the adjustment of the setup are mounted outside the VDS vessel. The transition from UHV to atmospheric pressure is provided by a bellow of stainless steel welded on the target arm. The target arm connects the target fork which holds the target wire, with the motion stage outside the vacuum.

Fig. 7 shows photo of the latest version of the target fork. Each target fork (Fig.7) is equipped with one wire or ribbon. To have a well defined target position with a straight orientation the targets are tensed on the target fork. The target-wire is tightened at the ceramics front, where the endswitch is mounted on the left-side part of the fork. The cables connecting the target and charge integrators as well as those connecting the endswitch and the target controller are used to feed the signals from UHV to the outside world. The body of the target fork is made of aluminum, while for the fork's arms marcor is used to insulate the target from the setup.

The target arm is mounted on a motion stage (Fig. 6 which provides a precise radial movement at a full path-length of about 40 mm, allowing to retract the targets to a secure position. This is necessary during injection when an rms beam width gets of about 2 mm (instead of 0.5 mm at normal running condition). The mechanical stability of the motion stage has been subject to

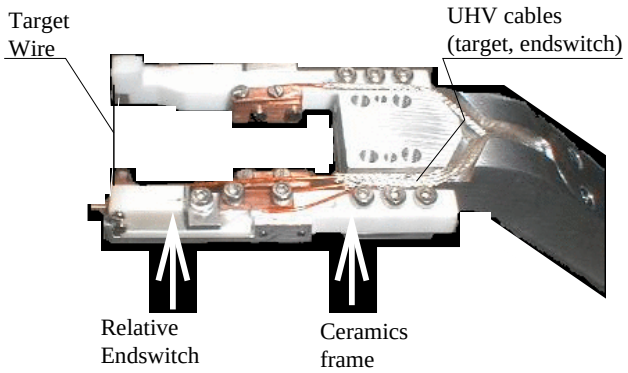

Fig. 7. *Target fork assembly.*

intensive studies [24,25] with a conclusion that the targets could be moved almost linearly with a precision in the order of 1 μm. This allows to calculate the position of the target from the number of steps the motor was driven, thus avoiding an independent measurement of the target position. However, a precise reference position is needed to calibrate the position measurement. This is provided by the end-switch mounted on the linear stage.

Fig. 8 shows schematically the structure of the relative endswitch. The switch opens whenever the target is fully retracted to its parking position; its precision is around O(1 μm), allowing the calibration of the target position with a high accuracy.

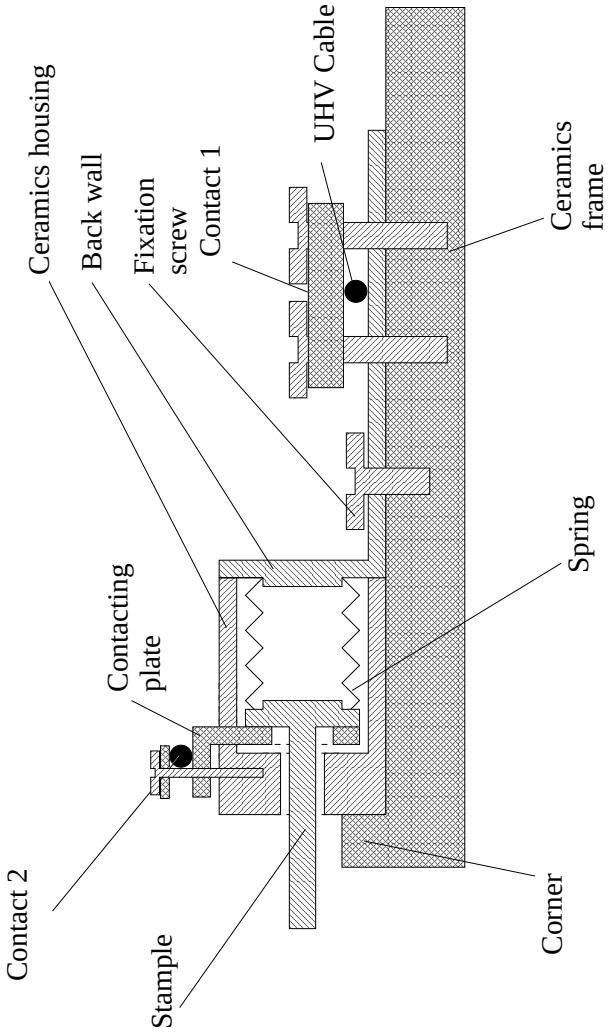

Fig. 8. *A scheme of the relative endswitch.*

To allow a stable target operation even if the beam is several millimeters off its design position, the target mechanics is built such that each target can be moved beyond the design beam position by 4 mm. Therefore opposite targets overlap in the radial range they cover. To avoid mechanical damage by an accidental collision of opposite targets, another end-switch was installed directly on each the target forks. The inner-end switch opens whenever an opposite target gets in contact with it. Like the outer end-switches they are connected to digital inputs on the target controller, so that the target steering system can react if a collision impends.

To successfully operate the target setup, an alignment of the target positions

must be ensured. This is done in few steps:
- an optical verification by estimating the distance between the targets and the target cage (precession - 1 mm). After evacuating the VDS vessel all targets have to be readjusted due to the atmospheric pressure impact.
- calibration and monitoring of the target operation through a window in the vertex vessel by means of CCD viewing system [24]. Resolution of the camera system is 768x568 pixels. One is able to calibrate the radial position of two opposite targets within 0.1 mm.
- reconstruction of primary vertices by VDS allows a further improvement of the calibration of the radial (50 μm) and longitudinal (500 μm) target positions.

At the first step the distances (Z-positions from the VDS entrance window, distances between initial positions of the opposite forks, relative distances between the opposite targets at the end-switch acting points) are measured. After the first step the single target operation is allowed and the second alignment step is made. It is based on comparison of actual target position (measured by an optical and mechanical devices) and position of vertices reconstructed in the VDS co-ordinate system. Typical X(Y) resolution is about 60 μm. Z-projections of vertices for the targets have resolution in the range of 550 μm. The second step gives the possibility to calculate eight target alignment constants $R_iVDS = R_iT + C_i$ needed for the radial target positions in the VDS detector. Now the multi-target operation is allowed and the Beam Position Monitor (BPM) data could be calibrated at the next alignment step. By multi-target runs two alignment constants ($X0$ and $Y0$) are calculated for the BPM center position: $X(VDS) = X(BPM) + X0$ and $Y(VDS) = Y(BPM) + Y0$, respectively. Since step 3 is made the distance between targets and the beam is evaluated using target stepping motors and the BPM data stream. The routine VDS movement IN or OUT combined with a temperature variation introduces additional small corrections (few μm) to the 8 target alignment constants. These corrections (step four of the Target alignment) were provided for each individual run. Target mechanics after its update was operated successfully during 2002-2003 data taking period having demonstrated a designed performance without any failure.

3.2 Target Data Acquisition System (DAQ).

To monitor and to measure the interaction rate, background as well as the HERA – B luminosity the Target DAQ together with Target Control System) has been built [26,27]. The overall interaction rate and the background was monitored by a set scintillation hodoscopes, silicon telescopes and Metal Foil Detectors (MFD) [28] mounted at different places of the HERA-B detector (1.

Each of scintillator hodoscopes as well as silicon telescopes consists of a pair of counters of different sizes. In total, at different periods of the data taking time the Target DAQ supported operation of 64 scintillation counters, 24 silicon detectors and 20 charge integrators. The coincident rate of each pair of scintillation or silicon counters was read-out by the Target DAQ scalers providing the following information about:

- the overall interaction rate
  - HERA-B 'Trigger Ring' - 12 scintillation hodoscopes (≈ 85 % acceptance) (located at the exit window of the VDS as shown in Fig. 9)
  - 8 scintillation hodoscopes with small geometrical acceptance (located at the position of the RICH sub-detector)
  - 8 silicon pad detectors (mounted at the exit window of the VDS vessel
  - 10 Metal Foil Detectors ring (replacing the scintillator 'Trigger Ring')

- individual target interaction rate
  - 8 silicon telescopes mounted inside the early version of a target arm
  - 8 charge integrators connected to the targets.

- background
  - 10 scintillation hodoscope (VETO-counters) placed 8 m in front of the experiment
  - 4 Metal Foil Detectors (mounted at VDS entrance window).

Large acceptance ($\approx$ 85 %) hodoscopes, 'Trigger Ring', were used for the interaction rate calibration, yet could not be applied for the targets steering due to their saturation at high rates (more than few MHz). The hodoscopes with a small geometrical acceptance (0.2 % per counter) mounted at the position of the RICH subdetector allowed to reliably calculate the luminosity even at high interaction rates O(100 MHz). The correction factors were determined and applied to the coincidence rate of every pair of scintillation counters in 'OR' mode for all 4 hodoscopes to get an absolute value of the interaction rate. That rate was used for the targets steering to keep the overall Interaction rate at the requested level or to generate the emergency signal in case if the interaction rate jumps up to prohibited level. Due to the small acceptance of the hodoscopes their reliable performance was guaranteed at the interaction rate up to 1 GHz. Yet, concerning the luminosity calculation the uncertainties arise due to the essential dependence of the hodoscopes acceptance upon:

- the target atomic mass;
- material distribution inside the HERA – B detector;
- beam position
- magnetic field;
- aging;

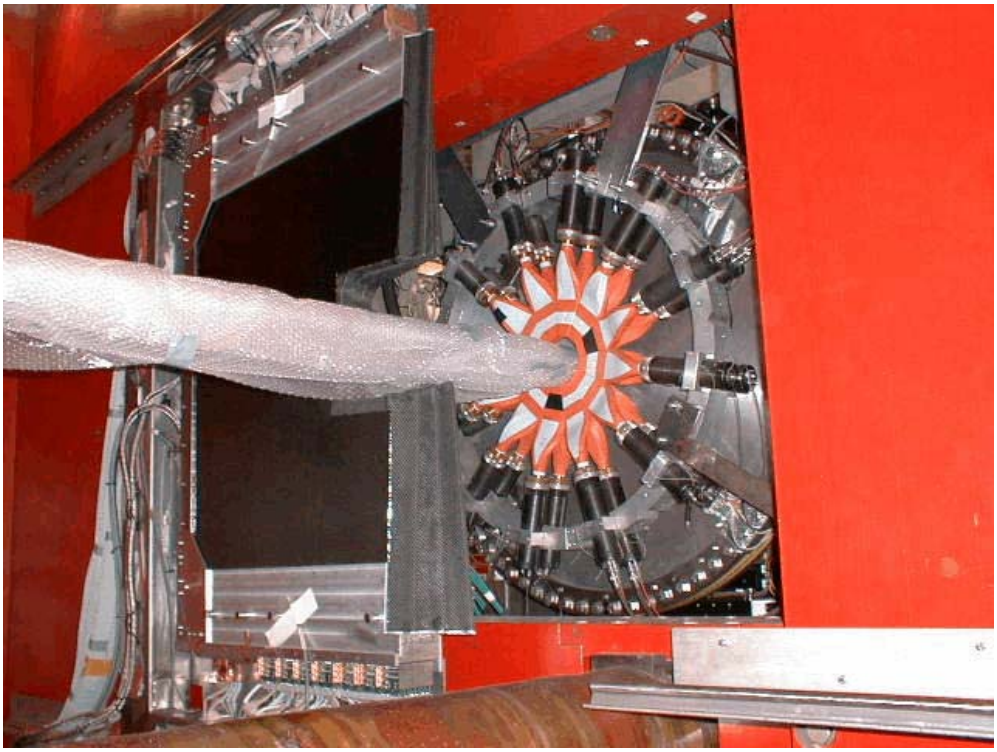

Fig. 9. *HERA-B Trigger Ring - 12 scintillation hodoscopes fixed at the exit window of the VDS vessel to monitor the overall interaction rate and/or the individual target contribution by the asymmetry method [8,25].*

- radiation damage;
- background contribution.

Altogether this makes Monte-Carlo uncertainty of the acceptance for these counters at the level of 50 %. To cross-check the hodoscopes performance related to the luminosity monitoring an additional set of four scintillation hodoscopes (acceptance 7%) and 10 Metal Foil Detectors (acceptance 49 %) were running permanently. MFD response is linear to the interaction rate and does not depend upon its time structure (scintillator counters produce a single count if two or more interactions occur during the same bunch crossing). An application of the MFD Luminosity Monitor for the comparison of acceptance of different parts of the HERA-B detector for different targets is illustrated in Fig. 10. The Fig. 10 shows dependence of the Up-Down vs Left-Right asymmetries for different targets. As one may see, there is an essential difference of the detector acceptance for different targets (up to ≈ 7 %). There is a bias by 22 % for the Left-Right asymmetry and 8 % for the Up-Down asymmetry. The origin of this bias most of all belongs to the non-axial beam position.

From the experience of exploring MFDs for the charged particle flux monitoring at HERA-B one may underline their main advantages [28] :
1) Extremely low mass of the detecting material.

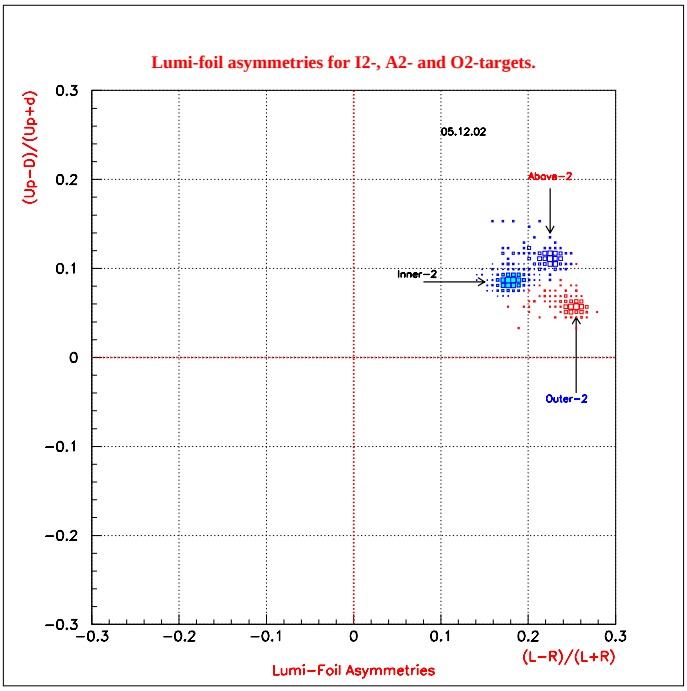

Fig. 10. *The asymmetries measured by the Up-Down and Left-Right sectors of the Metal Foil Detector monitoring ring.*

2) Simple structure (thin, up to few tens nano-meter, metal foils supported by the isolating frame).
3) Low operating voltage (20 V), which provides nearly total charge collection.
4) Simple read-out electronics (charge integrators and scalers).
5) Very high radiation tolerance.

Detailed analysis has shown that the luminosity measured by the scintillation counters matches the luminosity determined by other methods within 10%.

Background or VETO counters placed in front of the experiment provided monitoring of the non-target contribution into the interaction rate. The maximum levels of the background were set and included into the TaCoS (see section 3.3) to retract targets in the emergency case. Their values served also as a feedback data for tuning a beam and/or collimators.

The information about the timing of the interaction and the contribution of individual bunches (see an example in Fig. 2) was provided by measuring time spectra of scintillation hodoscopes by means of a TDC- and a FADC- setups [15,17,18].

For providing feedback data for the multi-target operation Silicon PIN-diodes positioned in target tubes in close vicinity to the target were tried first. There

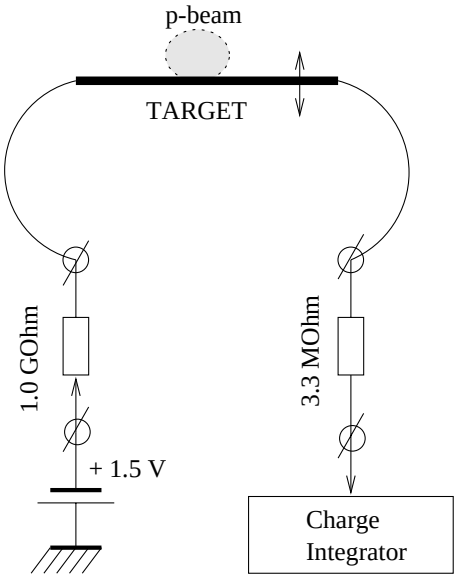

Fig. 11. Charge Integrator connections to the Target. Calibrating current from the stable source is fed through a target to the ChI input.

were difficulties, yet, to run the opposite targets due to superimposed contributions. Much more successful was a finally adopted concept of the charge integration in the electrically isolated targets. The individual contribution of each target was measured by sensitive Charge Integrators [29] designed and built for the HERA-B applications.

For the purpose of the charge integration all HERA-B targets are made out of the conductive wires. They are individually connected through the UHV feedthroughs to Charge Integrators (ChI) [29] housed in the NIM crate 5 m away from the targets. The Charge Integrator connection to the target is sketched in Fig.11. To suppress an impact of the external r/f sources the analog signal is converted inside the charge integrator into the output frequency ($\approx$ 100 Hz per 1 pA input current). The calibrating current from the stable source permanently flows through the target to the Charge Integrator allowing for to check the stability of its operation as well as to know the status of the target (partially broken target arriving into the beam, for instance). The conversion coefficients (ratio of the ChI output frequency to the Interaction Rate) for different targets were measured in a single-target calibration runs. Fig. 12 shows an example of the calibration plot for different targets illustrating a linear dependence of the charge integrators response on the interaction rate measured by the hodoscopes. The response of the ChIs to the IR cerated by a target (Fig. 12) is different even for the same target material (like carbon for the targets 'Inner2' and 'Below2'). This difference depends on the impact of the target orientation, proton beam profile, target surface, integrity of the target, background contribution, etc. That is why the calibration data were taken on a regular basis to keep calibration constants used by the TaCoS for the multi-target steering properly updated.

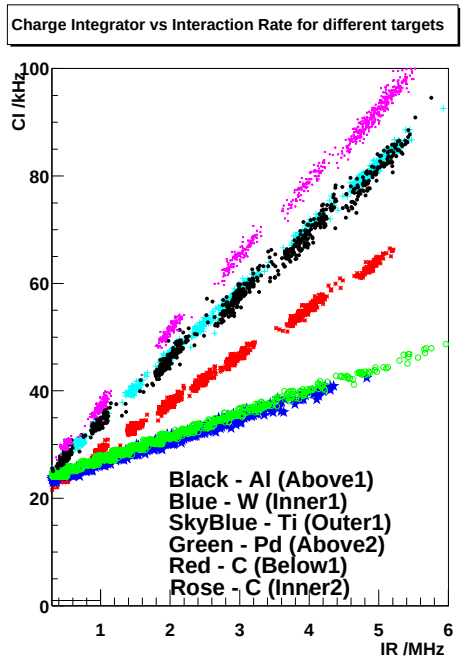

Fig. 12. *Linear response of the Charge Integrators to the interaction rate for the different target material.*

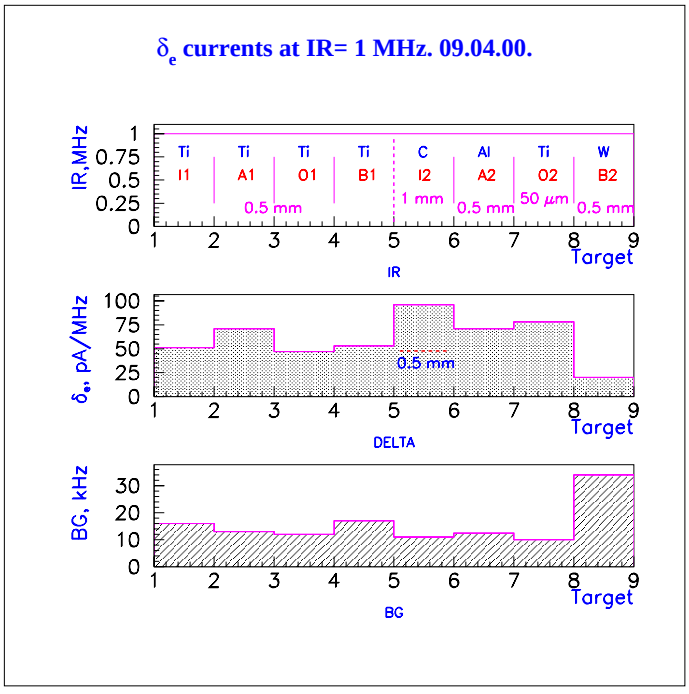

Fig. 13. *Specific currents for the different target material.*

Simulations of currents due to the δ-electron emission only [20] resulted in values few times less than observed, which supported the understanding that major part of the measured current was due to the low energy secondary electrons [28]. Specific currents (the target current corresponding to 1 MHz interaction rate) calculated on the basis of known values of the calibrating

current through every target ($\approx$ 250 pA) are shown in Fig. 13 together with a corresponding background level measured by the VETO - counters. Specific currents do not depend upon the ChI sensitivity (which was changed in course of the ChI modifications by few orders of magnitude).

While scintillating counters are sensitive also to the non-target background, Charge Integrators respond to the individual target-beam interaction, only. It was observed that hodoscopes could have omitted huge spikes in the IR (a saturation of the photo-multiplier last dinodes). If not accounted properly this might lead to the wrong determination of the delivered luminosity. Charge integrators respond linear to the interaction rate spikes up to 250 MHz. Well calibrated chareg integrators served also for the cross-check of the Luminosity monitoring.

3.3 Target Control System.

To provide a fully automatic operation of the target the Target Control System (TaCoS) has been developed. User interaction is limited to choosing the interaction rate and the desired target configuration only.The most important features of TaCoS are the following:

- insertion and retraction of targets.
- stabilization of the interaction rate;
- equal distribution of the interaction rate over the operated targets;
- emergency handling (to prevent the target system and the detector from being damaged by unintentionally high rates);
- an easy to communicate graphical user interface.

The main feedback signals for TaCoS are provided by the overall interaction rate measured by hodoscopes and partial interaction rates measured by the charge integrators. In an $\approx 10\ Hz$ steering loop TaCoS compares these rates with the anticipated ones given by the user. If the rate is too small the targets are moved closer towards the beam center, in case the rate is too large TaCoS retracts the targets. A proper step-size is calculated internally using a set of predefined parameters and the actual relative rate deviation. The actual configuration is sketched in Fig. 14. The system is subdivided into several modules running simultaneously and independently in a multi-threading environment. The modules exchange data via exclusive accesses to a global data buffer.
The system is controlled by the 'State Machine' module which handles each target independently from all others. Each target covers a well-defined state provided by the state machine and transitions between states follow well-defined rules. Thereby it is guaranteed that each state transition – often after having gone through several intermediate states – ends up with the system

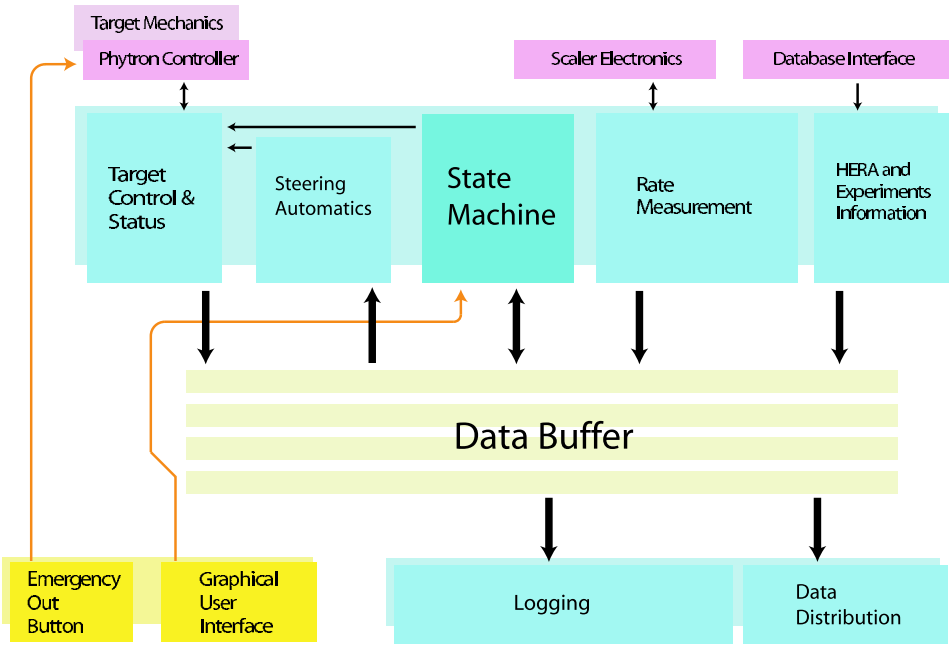

Fig. 14. *Simplified sketch of the target control system.*

being in a well-defined final state.

The 'Steering Automatics' module is responsible for stabilizing the interaction rate, whereas the rate measurement including the electronics readout is provided by the 'Rate Measurements' module. The 'HERA and Experiments Information' module delivers information on relevant collider parameters and on backgrounds at the other experiments. All data are stored to database by a logging module, and relevant data is sent to the HERA – B data acquisition system via an internal message system.

The 'Target Control And Status' controller module deals with the steering of the targets. It communicates with a programmable hardware controller (type Phytron) via serial line. The Phytron Controller receives move-commands from the controller module and actually drives the stepper motors of the target mechanics. It sends back the actual target positions and information on the status of the relative and outer ends-witches.

The TaCoS handles any emergency situation with the highest priority and starts to retract the targets as soon as any spike in the rate occurs or any failure inside the system is detected. In case the data exchange between the Phytron Controller and the controller module is interrupted, the Phytron Controller automatically retracts all targets to their end-switches. The same is true if the hard-wired emergency-out button is pressed. This provides the maximum possible security in case of computer problems. Another security aspect affects the protection against unintentional high rates. Spikes in the interaction rate are handled by an efficient emergency system: if the interaction rate exceeds

a given threshold (usually 60 MHz), all operated target targets are retracted by 20 μm (or by 200 μm if the rate exceeds 100 MHz). The TaCoS uses the background rate measured by a setup of scintillating counters upstream of the experiment to detect background emergency situation.

Any user input, like selecting targets and choosing the desired interaction rate, is done via a Graphical User Interface. It provides easy access to the control system and a concise display of the essential parameters and the measured values. Data exchange with the control system is done by means of the network protocol UDP.

Beam position is monitored regularly as well as rate fluctuations in different time regimes together with a frequency analysis of recorded rate time series/samples. An external data (HERA and other experiments etc.) are read from various online data servers, stored in online databases and used for monitoring and (if needed) correction in the target system operation. The online monitoring is very essential, for the operation of the target as well as for the coordination with other groups. All rate information together with the target positions are stored in online database servers.

3.3.1 Single-Target Operation.

The main task of the target control system is to keep the interaction rate stable, and to distribute it equally among the operated targets. The algorithm is built on top of a classic feedback-loop: the target steering reacts on fluctuations of the measured interaction rate. If the currently measured rate R is lower than the desired one (R_{auto}), the targets are moved towards the beam center. In case the interaction rate is larger than R_{auto}, the targets are retracted. A typical movement takes $O(10^{-2})$ s; in order to come to a steady state after each feedback cycle, the sampling time for the rate measurement has been chosen to 0.1 s, resulting in a feedback loop with a nominal cycle of 10 Hz.

Since feedback loops need 5-10 cycles to compensate for fluctuations [], the rate can be kept constant on a 1 s time scale only, while the compensation of shorter-term fluctuations needs other measures (cf. [30]). These intrinsic short-term fluctuations account for 6%-8% [20]. Since they cannot be compensated by the automatics, target steering is done only if the interaction rate differs from the desired rate by more than $\pm\Delta R$, $\Delta R/R = 10\%$ usually. This reduces unnecessary movements significantly. Additionally, to move the targets in, the averaged rate $\bar{R}$ of the last 5 measurements is asked to be smaller than R_{auto}, and larger than R_{auto} to move them out, respectively. That is,

- move the targets towards the beam, if

$$\bar{R} < R_{\text{auto}} \quad \wedge \quad R < R_{\text{auto}} - \Delta R \tag{6}$$

- retract the targets, if

$$\bar{R} > R_{\text{auto}} \quad \wedge \quad R > R_{\text{auto}} + \Delta R \tag{7}$$

The distance to move depends on the gradient of the proton density at the target position as well as on the target shape. This, so-called edge steepness, can be determined by measuring the response of the interaction rate to a well-defined single-step movement of the target towards or away from the beam. An example is shown in Fig. 15. Different step-sizes from -30 to +10 μm were performed, starting always at a rate of 10 MHz. The edge steepness shows an exponential profile; the fit results in a doubling of the rate by moving the target by 10 μm towards the beam [20].

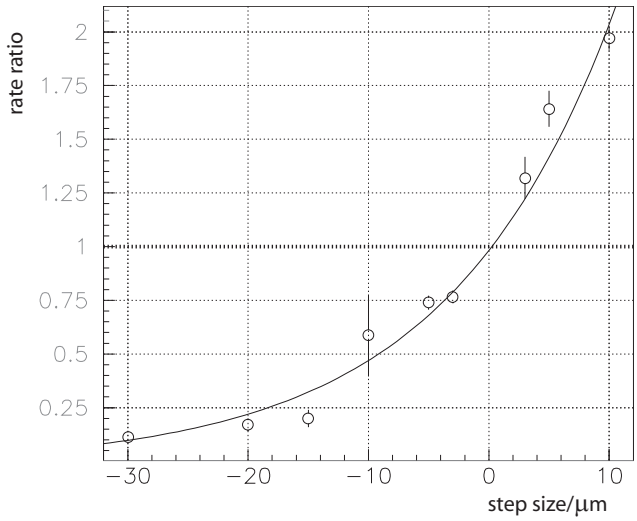

Fig. 15. *Steepness of the proton density. A 10 μm-step affects the interaction rate by factor of $\approx$ two.*

The steering automatics uses a simple ansatz for calculating the necessary step size to compensate rate fluctuations. Based on the results shown above, the target is moved by 0.1 μm per percent rate difference. For safety reasons, the maximum step size is limited to 5 μm, or rate changes of $\approx 43\%$.

3.3.2 Multi-Target Operation.

Different methods have been proposed and tested to provide a distribution of an interaction rate among the inserted targets [8]. Three of them were implemented in the MTS and tested in details: mechanical approach, silicon telescopes and charge integrators. Silicon telescopes mounted inside the target

arm were designed to measure the individual target contribution by the coincident rate of the two silicon pin-diodes oriented onto the specific target. The data obtained with the silicon telescopes have demonstrated that the straight-and-forward method of the multi-target steering based on a simple mechanical algorithm (sequentially moving in- or -out targets to keep the required rate stable) is by far not efficient. Individual contributions into the interaction rate even from two operated targets (measured by the silicon telescopes) were not equalized during most of the operating time.

The TaCoS steering of two targets using the data from the silicon telescopes was much more efficient: a smooth rate, equally distributed over the targets, actions by the TaCoS were in the right direction and faster. Yet, the irradiation impact onto silicon sensors was such that one needed once per a week to tune the hardware and make calibration to keep a good performance of the multi-target steering. Steering of more than two targets needed even more additional effort due to background contribution into individual telescopes rate from other operating targets.

Much more reasonable results were obtained with a method of the integration of the charge (see p. 16-19) borne in a target by the beam-target interaction (due to the Secondary Emission Electrons, mainly). This mmethod was implemented into the final construction of the internal MTS [31].

4 Operation Experience

The Multi-Target System was in operation during 1997-2003 year of the HERA – B experiment commissioning and running. The requested rates ranged from 0.5 up to 50 MHz at different multi-target configuration. In this section we illustrate the MTS performance with respect to its main characteristics: overall and shared rate stability, monitoring of the bunch population and luminosity.

4.1 Steering conditions and beam properties

In accordance with a basics requirements (cf. Section 2) the internal MTS consists out of eight thin ribbons or wires (Fig. 16), operated in the proton beam halo. The analysis shows that the various targets were usually operated at a distance of 3 - 5 rms beam width from the center of the beam (Fig. 17). The typical beam size of the proton beam at the target wires is characterized by σ_x and σ_y with a value of ≈ 400 μm. The main reason for the observed differences in a distance between the beam center and operated targets is the

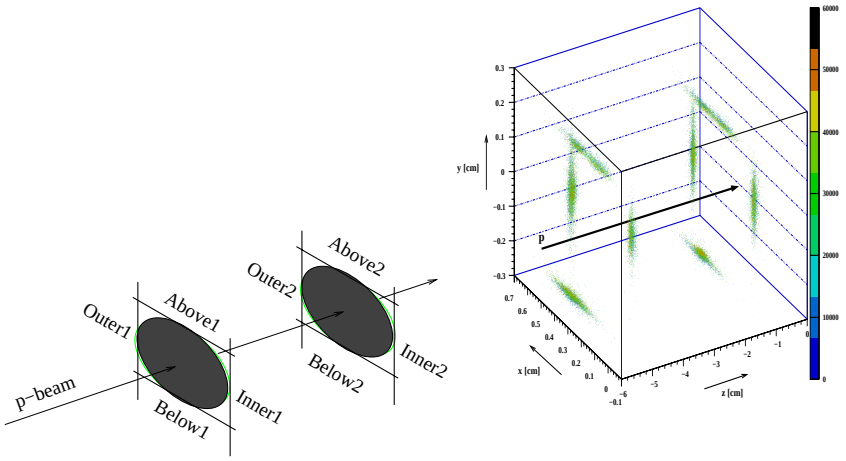

Fig. 16. *Schematic drawing (left) of the eight target wires surrounding the HERA proton beam and reconstructed vertices (right) while all eight target wires are operated simultaneously at the beam.*

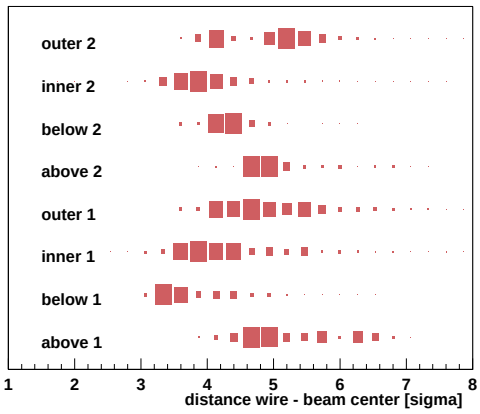

Fig. 17. *Distance between the beam center and targets operated during the year 2000.*

coasting beam contribution [14] which creates a broad transverse tail on the outer and above sides of the beam. Similar differencies were established for 'the beam-found' distance, which is defined at the first significant increase of the interaction rate when the target moves into the beam. The mean value of this distance ($\approx 6.5\ \sigma$) is determined by the HERA proton beam aperture limitation. These tight aperture limitation reduces the target efficiency and causes a rate instability.

A study has been carried out to reveal the sensitivity of the multi-target operation. Fig. 18 illustrates the MTS steering performance for the case with two targets ('Below-1' and 'Inner-1') in operation providing stable rate of 10 MHz. While the 'Below-1' target has been manually retracted in small steps of $\approx$ 10 μm out of the beam the steering automatics was steadily moving the 'Inner-1' target into the beam to keep the overall rate at the level of

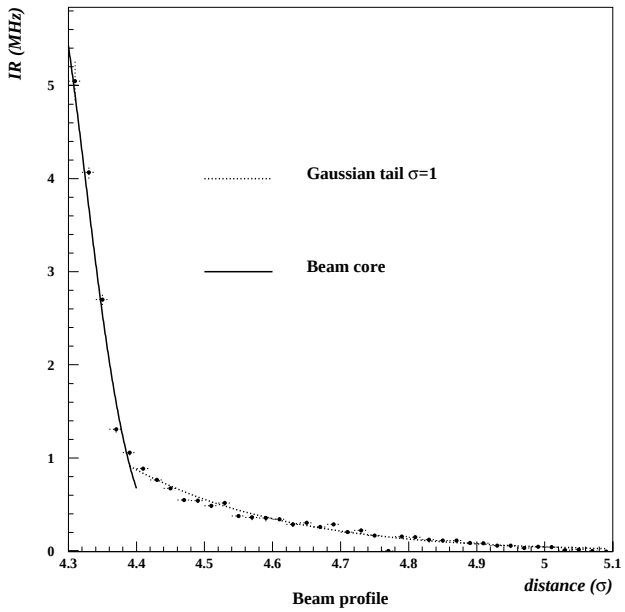

Fig. 18. *Interaction rate produced by the 'Below-1' target as a function of its distance to the beam core during a two-target operation requiring a constant overall rate of 10 MHz.*

10 MHz. The contribution of the 'Below-1' target dropped steeply from the initial 50 % (5 MHz) to 10 % already after the first four steps. This reveals the same sensitivity of the multi-target operation as in case of the step function measurements (Fig. 15) made with a single target operation.

4.2 Rate Stability

The interaction rate fluctuations lead to an enhanced probability for events with less and more interactions than aspired. The low multiplicity events reduce directly the statistics and the high multiplicity events are usually rejected within the trigger or reconstruction chain, causing a loss of the running efficiency.

The measured rate fluctuations depend on the chosen frequency or time range [30,20]. Fig. 19 shows short term fluctuations σ_s (obtained per each half of an hour of stable target operation) for the complete run period in the years 1999 and 2000 as a function of the time within a week. The target rate gets much more unstable during usual working hours, i.e. Monday to Friday between 7h and 16h, revealing a strong impact of civic noise on the target performance. The level of the observed rate fluctuations is compatible with what one expects from the beam orbit fluctuations. Extreme case correlated with an increased ground motion has been observed [27,30].

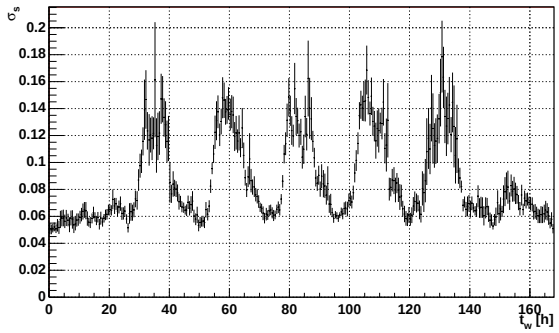

Fig. 19. *Short term rate fluctuations σ_s during the run period in the years 1999 and 2000 plotted versus the time in hours of a week (starting on Sunday 0h up to Saturday 24h).*

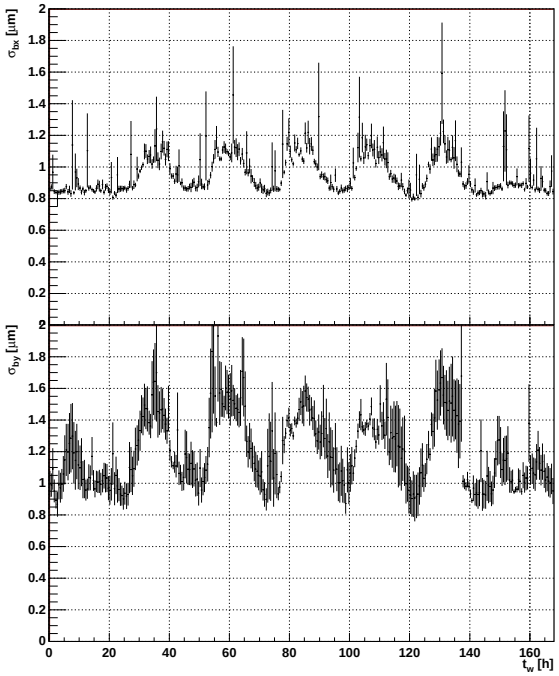

Fig. 20. *Short term beam orbit fluctuations σ_s for the same run period as in Fig. 19. Upper plot - horizontal: Bottom plot - vertical.*

The rate stability depends on the target orientation, material and shape. It is sensitive to beam orbit fluctuations as one may conclude from comparison of Fig. 20 and Fig. 19. Short term rate fluctuations (Fig. 19) follow exactly the beam orbit fluctuations (Fig. 20). It is well established that horizontal targets ('Above' and 'Below') reveal 2 times higher rate fluctuations than the vertical ones ('Inner', 'Outer'). This is correlated with the larger beam fluctuations in the y- direction compared to the x- one (Fig. 20 - bottom plot).

Concerning the target material, the tungsten produced the largest rate fluctuations. This is due to the large scattering inside the heavy target material which leads to a lower target efficiency ϵ_T. With respect to an impact of the

shape of the target the cylinder wires produced the least rate fluctuations. Targets with a poor surface (like carbon Inner-2 -target) revealed another interesting effect: the conversion coefficients for their charge integrators grown up by factor of two after being exposed to the atmosphere pressure (maintenance periods with flashing up the vacuum vessel by a dry nitrogen). They acquired their 'running condition' value after being in vacuum for ≈ 20 hours. This is explained by the dependence of the yield of the secondary electron emission on the surface status ([28]). We conclude here that targets manufactured out of lighter material and with rough surface or with a cylinder shape enables a smoother beam scraping and as a result provide more stable rate.

Another known reason for teh reduction of the running efficiency is a bunch population. The monitoring of the bunches population has revealed that the longitudinal proton beam properties were not optimal. One observed side-bunches of the 208 MHz system which accounted for approximately 10 % of the target interactions [9,18]. Another 'timing' problem was caused by coasting beam protons [14,19,9,27,10]. Especially on the outer and above targets a significant amount of un-bunched coasting beam contribution was established. Protons with an energy deviation $|\Delta E/E| > 2...3 \cdot 10^{-4}$ start to cross the separatrix in the longitudinal phase space and travel now freely (un-bunched) around the proton ring. At HERA one usually just observes protons with negative energy deviation, the main reason for that are presumably the energy losses due to synchrotron radiation which accounts for approximately 10 eV/turn. Due to the negative dispersion D_x in the target area these protons are displaced in the horizontal phase space to the outer side: $\Delta_x = D_x \cdot \Delta E/E$ m. One observes in the vertical direction also a negative spurious dispersion $D_y \approx -0.2\ m$, causing a shift of the coasting beam protons to the above side. The production mechanism, which forces the protons to cross the separatrix is not finally understood, while potential reasons could be discussed: Intra Beam Scattering, RF noise, energy loss inside the target etc. The TaCoS performance for the case of four targets operating in the beam to produce 40 MHz interaction rate is illustrated in Fig. 21. As one might see the MTS steering works perfect making targets to follow precisely the beam movement which was measured by the HERA – B Beam Position Monitors (their position is indicated in the 1): the beam step in the X - direction at time around 26 h is well followed by the steps in the evolution of the INNER-1 and Outer-1 targets (naturally in opposite directions) at the same time. Similarly, the beam step in Y - direction at the time around 27 h is followed by the corresponding steps (again in opposite directions) by the ABOVE-1 and BELOW-1 targets. The path of the targets position is well confirmed by the primary vertices distribution reconstructed by the VDS analysis tools.
The TaCoS keeps the interaction rate stable even at comparatively large fluctuations in the beam position (Fig. 21- time between 25.7 and 26.4 h). Yet, there are also ranges in time when the rate fluctuations are not well com-

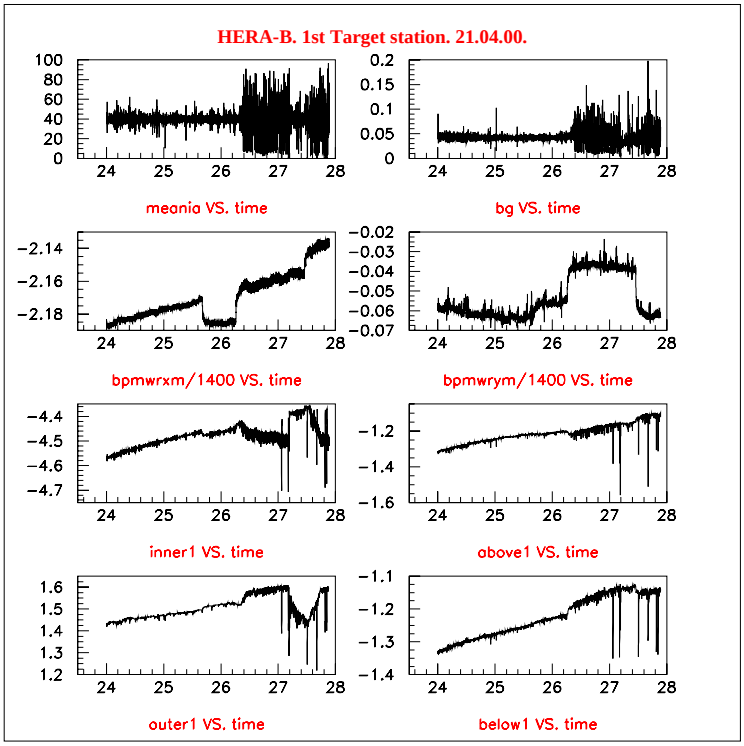

Fig. 21. *Four targets operation. Upper plots: Interaction (left)and background (right) rates as a function of the time (in hours). The beam position progress is depicted in the second raw of plots (X-axis -left plot, Y-axis - right plot). The plots at the third and fourth raw show the targets position.*

pensated. The possible reasons for the rate instability were addressed in the previous section.

4.3 Multi-Target Operation

As it was discussed the relative target contributions are well controlled by the charge integrators. The Fig. 22 shows for 4 inserted targets the distribution of primary proton interactions. The reliability of the interaction rate distribution by charge integrators has been verified by reconstructing the distribution of primary vertices on the targets by means of the HERA-B vertex detector [23]. The relative number of vertices on each target is in a good agreement with the partial interaction rate deduced from the ChI rate [13]. It is established that the error in the relative luminosity provided by charge integrators does not exceed 5 %. An additonal proof of a perfect TaCoS performance in a multi-target regime with a feedback from the charge integrators comes out from analysis of the vertices distribution over the targets in comparison with Monte-Carlo expectation. The Fig. 23 shows the number of target-wires on which a vertex was found as a function of the total number of reconstructed vertices (upper plot - real data, bottom plot - Monte-Carlo simulation). The correlation

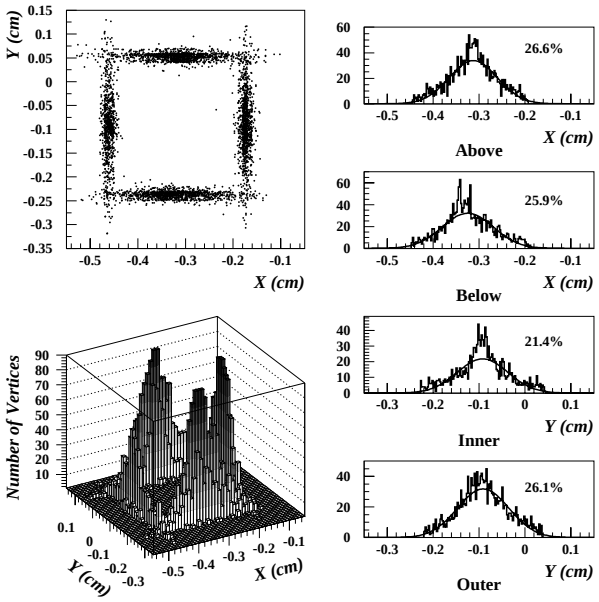

Fig. 22. *An interaction rate distribution equalized by charge integrators over four targets: Right: Charge distribution over 4 inserted targets. Left:Distribution of primary vertices on 4 targets reconstructed by the VDS.*

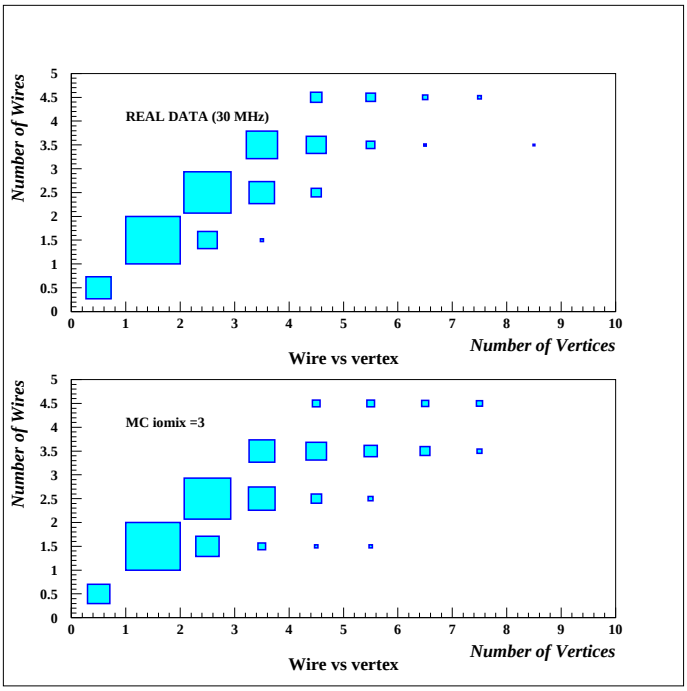

Fig. 23. *MTS operating four targets simeltaneously. Dependence of the number of target-wires on which a vertex was found on the total number of reconstructed vertices: upper plot - real data, bottom plot - Monte-Carlo simulation.*

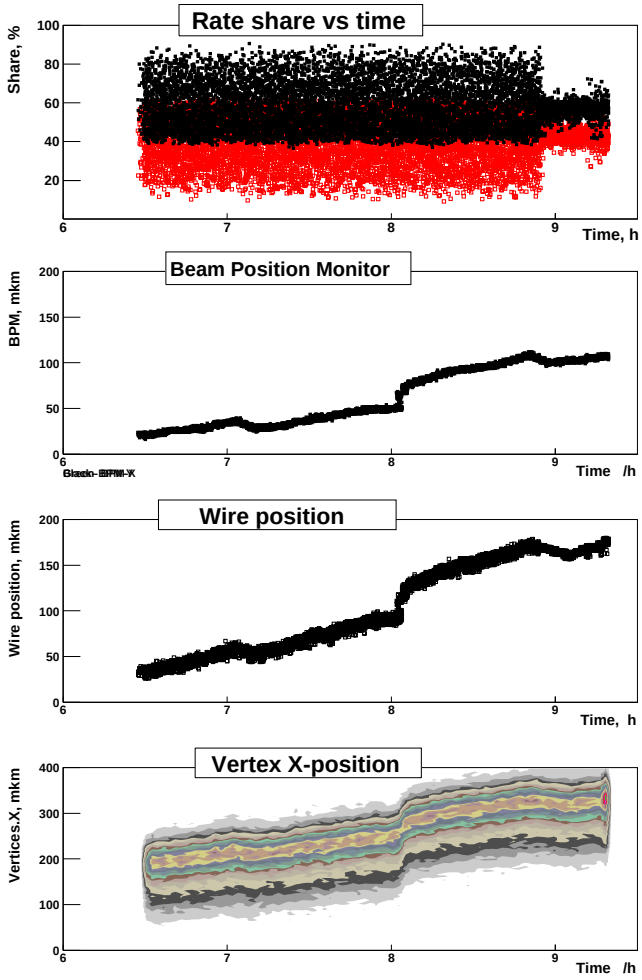

Fig. 24. *Rate sharing stability: Tungsten and Carbon. Upper plot: Interaction rates measured by the charge integrators as a function of the time (in hours). The beam and targets position progress is depicted in the second and third raw of plots. The bottom plot shows the primary vertices reconstructed by the VDS software.*

of the data in the same way at both plots indicates a very homogeneous distribution of ther interaction rate over all four targets. The Fig. 24 illustrates the rate sharing stability in a two-target (Tungsten and Carbon) run. The top plot shows that the rate sharing had at the beginning of the run rather big fluctuations which were significantly reduced at the end of this run by optimization of the steering parameters. The beam position (X - axis) monitor (second plot from the top) and target position (third plot from the top) are well correlated. The bottom plot shows the X coordinate of reconstructed vertices which reflects the target path. Thus, the MTS steering makes targets to follow the beam position progress keeping the overall rate as well as shared rates stable.

The luminosity L was monitored by counting the number of inelastic beam-target interactions exploiting the MTS counters. Using the relevant inelastic production cross section σ_{inel}^{pA} [33] one may calculate the luminosity produced by a single target with atomic mass number A:

$$L = \frac{\lambda \; N_{BX}}{\sigma_{inel}} \; , \tag{8}$$

with N_{BX} being the number of filled bunches and λ - the mean number of inelastic beam-target interactions per filled bunch. λ can be derived from the interaction rate R_{ia}^{hodo} measured by the MTS hodoscopes:

$$\lambda = \frac{K(A) \; R_{ia}^{hodo}}{R_{BX}} = \frac{K(A) \; R_{ia}^{hodo}}{8.523\,\mathrm{MHz}}. \tag{9}$$

Here, R_{BX} is the mean bunch crossing rate (from (1)), and $K(A)$ is a correction factor related to the geometrical acceptance of the hodoscopes dependent upon the target material, mainly.

To calculate λ different MTS counters (1) have been used. The data obtained agree within few % (see Table 3).

Detector	Interaction Rate [MHz]	Luminosity [mb$^-$1]
Hodoscopes	1.395	837.8
MFD	1.355	836.4
Charge Integrators	1.360	836.2

Table 3
Luminosities measured by different MTS detectors

The 'on-line' luminosity at HERA-B was monitored and measured by the MTS, while off-line analysis (using data from other HERA-B sub-detector systems: Electro-magnetic Calorimeter, VDS, RICH) was applied to cross-check the obtained results and introduce the necessary corrections. The luminosity determination for multi-target runs with mixed target material required taking into the cross-section and track multiplicity dependence upon the atomic mass A of the targets.

5 Summary

The first so far built multi-target setup inside a high energy proton storage ring has been successfully explored in the years 1997-2003 at the HERA storage

ring.
The advanced multi-target steering techniques has provided stable luminosity for the HERA – B experiment with its updated physics goal aimed at the study of the A-dependence of a heavy flavor production.
The luminosity has been delivered by up to 8 simultaneous interaction points with the overall interaction rate of up to 40 MHz equally shared by the targets operated in the proximity to the beam core, at progressively (or occasionally) changing parameters of the proton and/or positron beams as well as of the targets.
The Mechanics, Target Control and Monitoring Systems were able to stabilize the interaction rate within 10 % operating the multi-target setup during 90 % of the time available for the HERA – B experiment. No significant deterioration of the performance of other HERA experiments has been observed.

6 Acknowledgments

We express our thanks to the HERA Machine Group for the support and frank discussions. We are especially grateful to the following persons and their groups :F. Willeke and M. Seidel (DESY), K.T. Knoepfle, Ch. Bauer, N. Bulian, S. Schaller and J. Spengler (MPIfK, Heidelberg), M. Braeuer, G. Baki, T, Jagla (Dortmund University), Yu. Pavlenko, V. Kiva (KINR), V. Pereverтailo (Insitute of Microdevices, Kiev). We acknowledge the support from the BMBF (Germany), NAS and MES (Ukraine). Some of us (V. P., V. A., Yu. V.) thank the MPI für Kernphysik (Heidelberg) and DESY (Hamburg) for the support and generous hospitality.

References

[1] E. Hartouni et al., *An Experiment to Study CP Violation in the B System Using an Internal Target at the HERA Proton Ring*, Design Report, **DESY-PRC 95/01** (1995).

[2] A. Gruber et al., *Nucl. Inst. Meth.* **A282** (1989) 87

[3] V.F. Dmitriev, S. G. Popov, D. K. Toporkov et al.,*Phys. Lett.* **157B** (1985) 143

[4] HERMES Collaboration, *HERMES Technical Design Report* (1993)

[5] V. Pugatch et al., *Micropowder Jet Target for Storage Rings Nucl. Inst. Meth.* **B70** (1992) 570

[6] F. Hinterberger, T. Mayer-Kuckuk and D. Prasuhn, *Nucl. Inst. Meth.* **A275** (1989) 239; C. Tschalär, *Nucl. Inst. Meth.* **A308** (1991) 471.

[7] H.R. Koch et al., *Nucl. Inst. Meth.* **A271** (1988) 375.

[8] C. Hast et al., *Test of Internal Halo Targets in the HERA Proton Ring*, Nucl. Instr. Methods **A354** (1995) 224.

[9] The HERA-B Collaboration, *HERA-B Report on Status and Prospects, October 2000* DESY-PRC 00/04, 2000.

[10] G.H. Hoffstaetter (ed.), *HERA accelerator studies 1999*, **DESY HERA 00-02** (2000).

[11] M. Seidel, , **DESY** 94-103 (1994).

[12] E. Lohrmann and M. Seidel, *Study of Background Caused by Scattering at the HERA-B Wire Target*, **DESY HERA 95-04** (1995).

[13] V. Pugatch, K.T. Knoepfle, Yu. Vassiliev, *Beam Profile Imaging Target. Nucl. Phys.* **A 701** (2002) 204

[14] K. Ehret et al., *Observation of Coasting Beam at the HERA Proton-Ring,* Nucl. Instr. Methods **A456** (2001) 206.

[15] S. Schaller, *Untersuchung der Beiträge einzelner Protonbündel zur Wechselwirkungsrate des HERA-B Experiments,* Diplomarbeit University of Heidelberg (1998).

[16] S. Spratte, *Untersuchung zu den Eigenschaften eines internen Drahttargets für das HERA-B Experiment,* Diplomarbeit, University of Dortmund (1996), **DESY F15 96-01**.

[17] M. Symalla, *Vorbereitende Untersuchungen zur Bestimmung der Wechselwirkungsraten und deren Zeistruktur,* Diplomarbeit University of Dortmund (1999).

[18] G. Baki, *Untersuchungen der Wechselwirkungen einzelner Protonenbunche mit dem HERA-B Drahttarget*, Diplomarbeit, University of Dortmund (2000).

[19] S. Spratte, *Bestimmung der Wechselwirkungsrate des HERA-B Targets und Untersuchung des Coasting Beams am HERA Protonenring,* PhD Thesis, University of Dortmund (2000).

[20] S. Issever, *PhD Thesis,* **Dortmund University** (2001)

[21] T. Jagla, *Untersuchung der Target-Strahl Wechselwirkunge im HERA-B Target,* Diplomarbeit, University of Dortmund (1998), **DESY-THESIS 1999-007**.

[22] M. Funcke, *PhD Thesis,* **University of Dortmund** (2003).

[23] C. Bauer et al., *Nucl. Instr. Meth.,* **A418** (1998) 65

[24] M. Funcke, *Alignment der HERA-B Targetmechanik*, Diplomarbeit, University of Dortmund (1999).

[25] M. Bräuer, *Aufbau und Untersuchung der Eigenschaften des Targets für den HERA-B Detektor*, Diplomarbeit, University of Dortmund (1997).

[26] K. Ehret, *Performance of the HERA-B Target and Interference with HERA operation*, International Symposium on Near Beam Physics, FNAL Batavia, Proceedings (1997) 33.

[27] K. Ehret, *Commissioning of the HERA-B Internal Target: Using the HERA Proton Ring as a B-Factory*, Nucl. Instr. Methods **A446** (2000) 190.

[28] V. Pugatch et al., *Metal Foil Detectors and their Applications*, Nucl. Instr. Methods **A535** (2004) 566

[29] N.M. Tkatch, V.A. Kiva, *Scientific Papers of the Institute for Nuclear Research,* **No. 2(4)** (2001) 72

[30] Chr. Knierim, *Messung und Analyse von Ratenfluktuationen am HERA-B-Target*, Diplomarbeit, University of Dortmund (2000).

[31] Y. Vassiliev et al., *Multi Target Operation at the HERA-B Experiment*, STORI99, Bloomington, Indiana, US, (1999), Proceedings published: Nuclear Physics at Storage Rings 359.

[32] Chr. Knierim, *PhD Thesis,* **University of Dortmund** (2004).

[33] J. Carvalho, *Nucl. Phys.* **A725** (2003) 269